HHS Public Access

Author manuscript

Cell Rep. Author manuscript; available in PMC 2018 March 07.

Published in final edited form as:

Cell Rep. 2017 December 12; 21(11): 3040–3048. doi:10.1016/j.celrep.2017.11.065.

Integrating Extracellular Flux Measurements and Genome-Scale Modeling Reveals Differences between Brown and White Adipocytes

Alfred K. Ramirez[1,2], **Matthew D. Lynes**[1], **Farnaz Shamsi**[1], **Ruidan Xue**[1,^], **Yu-Hua Tseng**[1], **C. Ronald Kahn**[1,†], **Simon Kasif**[2,3,†], and **Jonathan M. Dreyfuss**[2,4,†,*]

[1]Section of Integrative Physiology and Metabolism, Joslin Diabetes Center, Harvard Medical School, Boston, MA 02215, USA

[2]Department of Biomedical Engineering, Boston University, Boston, MA 02215, USA

[3]Graduate Program in Bioinformatics, Boston University, Boston, MA 02215, USA

[4]Bioinformatics Core, Joslin Diabetes Center, Harvard Medical School, Boston, MA 02215, USA

Summary

White adipocytes are specialized for energy storage, whereas brown adipocytes are specialized for energy expenditure. Explicating this difference can help identify therapeutic targets for obesity. A common tool to assess metabolic differences between such cells is the Seahorse Extracellular Flux (XF) Analyzer, which measures oxygen consumption and media acidification in the presence of different substrates and perturbagens. Here, we integrate the Analyzer's metabolic profile from human white and brown adipocytes with a genome-scale metabolic model to predict flux differences across the metabolic map. Predictions matched experimental data for the metabolite GABA, the protein ABAT, and the fluxes for glucose, glutamine, and palmitate. We also uncovered a difference in how adipocytes dispose of nitrogenous waste, with brown adipocytes

[†]Co-corresponding Authors: C.Ronald.Kahn@joslin.harvard.edu; kasif@bu.edu; jdreyf@bu.edu.
[^]Deceased
[*]Lead Contact
Kahn and Kasif are listed alphabetically

Software Availability

The code to reproduce the modeling from this paper is provided at https://github.com/ramirez-a/Brown-White-FBA. The code and results for the preadipocytes' microarray analysis is at https://github.com/jdreyf/pread-brown-white. An R package to integrate Seahorse XF Analyzer data into the human metabolic model and generate flux predictions is provided at https://github.com/jdreyf/sybilxf.

Accession Numbers

Preadipocyte microarray data were deposited in GEO under accession GSE100003. Recon 2.1A was deposited to Biomodels (Chelliah et al., 2015) under accession MODEL1703310000.

Author Contributions

AKR, JMD, CRK, SK, MDL, and Y-HT wrote the paper. AKR, JMD, CRK, and SK designed the conceptual framework and analyzed the results. AKR, RX, and FS performed the *in vitro* experiments. AKR and JMD performed the *in silico* modeling experiments. AKR assembled the figures.

Competing Financial Interests

The authors have no competing financial interests to declare.

secreting less ammonia and more urea than white adipocytes. Thus, the method and software we developed allow for broader metabolic phenotyping and provide a distinct approach to uncovering metabolic differences.

Graphical Abstract

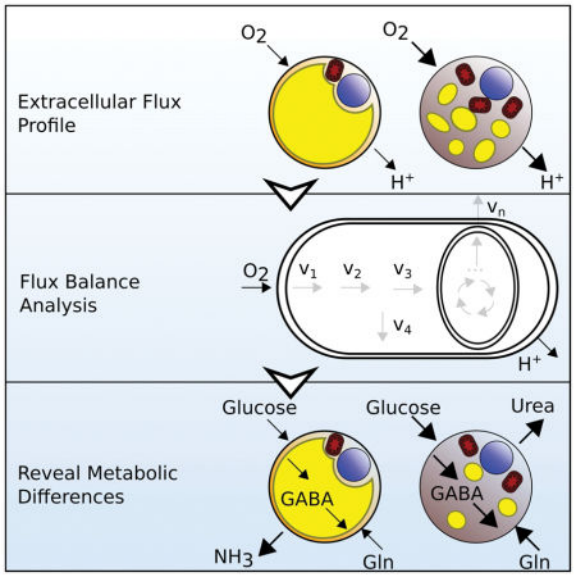

Introduction

Adipose tissue is critical for maintenance of metabolic homeostasis through its effects on energy balance and its endocrine function (Tran and Kahn, 2010). Adipose is capable of expanding and remodeling to meet a wide range of metabolic challenges by increasing the number, size and activity of adipocytes (Hyvönen and Spalding, 2014). Adipocytes can be broadly divided into three metabolically-distinct types: white, brown, and beige adipocytes (Giralt and Villarroya, 2013). White adipocytes are energy storing cells characterized by large unilocular lipid droplets (Tchkonia et al., 2013). Brown adipocytes have multilocular fat droplets and are involved in expending energy for thermogenesis via uncoupled respiration, which is mediated by the inner mitochondrial membrane protein uncoupling protein 1 (UCP1) (Cannon J., 2004). Beige adipocytes also express UCP1 and are found dispersed in white adipose depots where they can be induced to burn energy to generate heat like brown adipocytes (Sanchez-Gurmaches and Guertin, 2013). Although it had been thought that brown adipose tissue was present in humans only in infancy, we and others have shown that brown adipose tissue is present in adult humans and is correlated with lower BMI and lower fasting glucose levels (Cypess et al., 2009, 2013).

Activation of brown adipose tissue or increasing brown adipose mass in murine models has been shown to improve glucose metabolism, increase energy expenditure, reduce hypercholesterolaemia (Berbée et al., 2015), and protect against obesity (Harms and Seale, 2013). Similarly, activation of brown adipose in humans with type 2 diabetes via cold exposure can improve insulin sensitivity (Hanssen et al., 2015), and improved insulin

sensitivity is a feature of increased protection against diabetes and its complications and co-morbidities such as cancer, heart disease and Alzheimer's (Laakso and Kuusisto, 2014; Orgel and Mittelman, 2013). Pharmacological activation of human beige and brown adipose tissue is therefore being explored as a potential therapy for human obesity (Cypess et al., 2015), and it is critical to gain better insight into the metabolic differences between brown and white adipocytes to elucidate the full set of potential targets responsible for the beneficial effects of brown adipose tissue (Tseng et al., 2010).

The ideal method to characterize the brown and white adipocyte metabolic profiles would be via genome-scale experimental metabolic flux analysis, e.g. (Quek et al., 2010), but this is experimentally challenging. An increasingly popular technique to assess metabolic differences *in vitro* between cells of different types or in different conditions is to measure extracellular fluxes of metabolites like oxygen, carbon dioxide, and lactate. For example, the Seahorse XF Analyzer can be used to measure oxygen consumption rate (OCR) and pH change, which is read out as extracellular acidification rate (ECAR) or proton production rate (PPR), in the presence of different substrates or perturbagens to estimate mitochondrial respiration and glycolysis. The Seahorse Analyzer has been used in thousands of studies, including with isolated adipose tissue, preadipocytes, and adipocytes (Gesta et al., 2011; Xue et al., 2015).

Metabolic fluxes can be modeled *in silico* via a technique called flux balance analysis (FBA) (Orth et al., 2010). In this framework, each metabolite's input and output fluxes balance, i.e. equalize, so that the metabolite's concentration is steady. FBA represents a metabolic network with a stoichiometric matrix that captures the stoichiometric coefficients of each biochemical reaction as a column of the matrix, where each matrix row represents a metabolite. The fluxes are bounded by lower and upper bound constraints, respectively, that encode constraints such as reaction directionality and limited nutrient uptake. Together, the stoichiometric matrix and lower and upper bounds define the feasible flux configurations at steady state via linear constraints, which can be solved efficiently. Moreover, if a cellular objective, such as ATP synthesis, is postulated, it can be maximized subject to the constraints to yield an optimal flux configuration.

Genome-scale metabolic network models have been constructed for over 100 organisms, from bacteria to fungi to human cells (Dreyfuss et al., 2013; Feist et al., 2009). Some models have been made for specific human tissue and cell types. For example, the white adipocyte model iAdipocyte1809 has been used to elucidate metabolic differences between lean and obese states (Mardinoglu et al., 2014, 2013) and before and after weight loss (Mardinoglu et al., 2015). However, we did not use iAdipocyte1809 or its successor iAdipocytes1850, because we wanted to be able to uncover brown adipocyte specific metabolic reactions. Thus, we began with the human generic genome-scale metabolic model Recon 2.1x, an update to Recon 2 (Thiele et al., 2013) where all the reactions are elementally-balanced, which makes the model suitable for FBA (Quek et al., 2014; Sahoo et al., 2015; Smallbone, 2013).

Prior studies have shown the potential of connecting extracellular measurements with FBA (Aurich et al., 2015; Fan et al., 2013, 2014; Frezza et al., 2011; Kaplon et al., 2013; Mo et

al., 2009; Munger et al., 2008; Si et al., 2009), but thus far, FBA has not been systematically integrated with Seahorse Analyzer metabolic profiling to predict the full range of intracellular fluxes. Figure 1A illustrates that the Seahorse Analyzer directly measures several fluxes; by addition of chemical perturbations it indirectly measures several more (explained in Figure 1B); and, although only a selected few other fluxes are drawn, the rest of the fluxes stretching across the metabolic network can potentially be inferred from integration with FBA. In this work, we show that by integrating Seahorse measurements with genome-scale FBA we can infer flux differences in substrate uptake and, more importantly, across the metabolic map between white and brown adipocytes. We then compare these predicted differences to publically available data and measure selected predicted fluxes experimentally to identify differences in clinically and physiologically relevant metabolic pathways.

Results

Reconstruction and validation of the human genome-scale metabolic model Recon 2.1A

We began with Recon 2.1x and applied a series of tests to determine whether this genome-scale metabolic model would produce biologically feasible results for white and brown adipocytes, particularly with regards to central carbon metabolism and energy utilization. As we applied these tests, we found that we could improve upon Recon 2.1x to give more quantitatively realistic results. Therefore we implemented an iterative process from a reconstruction protocol (Thiele and Palsson, 2010) to revise Recon 2.1x and termed the final revised model, *Recon 2.1A*. For example, we tested if Recon 2.1x would produce biomass only in the presence of all essential nutrients by blocking external metabolites present in the Seahorse media one at a time. As seen in Figure S1, Recon 2.1x correctly predicted nearly all of these metabolites except phenylalanine, which is an essential amino acid (Figure S1C). We corrected this prediction in Recon 2.1A (Figure S1D). Other examples of our revision are that Recon 2.1A can produce realistic amounts of ATP given carbon sources of different lengths (Coles et al., 2013)(Figure S1E), and that Recon 2.1A supports flux through all the canonical fluxes of central carbon metabolism (Figure S2). Overall, these changes to the model (listed in Table S1) had a systemic impact on the flux bounds of thousands of reactions in Recon 2.1A (Figures S1A and S1B).

Integrating Seahorse XF Analyzer metabolic flux profiles with Recon 2.1A enables accurate assessment of flux differences

To generate metabolic profiles for brown and white adipocytes, we performed an oxidative stress test using the Seahorse XR24 Analyzer. Using medium containing glucose (25 mM) and several amino acids as substrates (Table S1), brown adipocytes had a basal oxygen consumption rate (OCR) 9-fold higher than white adipocytes (Figure 2A), consistent with their known differences in energy expenditure compared to energy storage (Xue et al., 2015). The basal proton production rate (PPR), a measure of glycolytic activity, was higher in brown adipocytes compared to white adipocytes (Figure 2B). The addition of pyruvate (1 mM) did not change OCR or PPR in either brown or white adipocytes. Based on the perturbation data, brown adipocytes had higher ATP production and proton leak compared to white adipocytes (Figure 2C). The spare respiratory capacity was 8-fold higher in brown

adipocytes than white adipocytes. Lastly, the non-mitochondrial OCR was 10-fold higher in brown adipocytes than in white adipocytes. We used these measurements to estimate representative normal distributions given a mean and standard deviation, and then sampled from these distributions to produce one set of constraints for brown adipocytes and one set for white adipocytes. For non-measured exchange fluxes, we estimated the upper bounds from empirical principles. For each set of sampled constraints, we then minimized total flux (Holzhütter, 2004).

Figure 2D–G shows the significant (FDR < 0.05) predicted flux differences between brown and white adipocytes for a carbohydrate (glucose), an amino acid (glutamine), a free fatty acid (palmitate) and a waste metabolite (ammonia). The model predicted higher substrate utilization in brown compared to white adipocytes for glucose, glutamine, and palmitate as well as higher secretion of ammonia, as a waste product of amino acid (arginine) metabolism.

To validate these flux predictions made by the model, we analyzed cells with the Nova BioProfile FLEX Analyzer, which assessed concentrations of seven extracellular metabolites (Figure S3). Consistent with FBA-derived predictions, uptake of glucose and glutamine was higher in brown compared to white adipocytes (Figure 2H and 2I). Similarly, previous measurement of palmitate uptake (Xue et al., 2015) using radiolabeled palmitate was shown to be higher in brown than white adipocytes (Figure 2J). While the metabolic model did not predict a difference for sodium and potassium uptake, uptake of both were significantly higher in brown than white adipocytes (Figure S3). The measurements for glutamate and lactate were below the instrument detection limit (Figure S3). Although the magnitudes of the predicted fluxes were different from the measured values, the pattern of predicted and measured fluxes was consistent (Figure S4). However, inconsistent with the metabolic model's prediction, white adipocytes had higher ammonia secretion than brown adipocytes (Figure 2K).

Brown compared to white adipocytes have lower ammonia secretion despite a higher metabolic demand

The difference in ammonia secretion between our experiments and the predictions by our model was unexpected. We therefore sought to identify the metabolic reactions responsible for this discrepancy. We first constrained the ammonia, glutamine, glucose, and palmitate fluxes to their measured values. We then matched the mathematical objectives to the known biology by using the different lipidomic profiles of brown and white adipose tissue (Hoene et al., 2014) to create brown and white-specific lipid objective functions. To construct these objectives, the lipids species were coalesced into 10 major lipid classes: ceramides, diglycerides, triglycerides, free fatty acids, phosphotidylcholines, phosphotidylethanolamines, phosphotidylglycerols, phosphotidylserines, phosphotidylinositols, and sphingomyelins (Table S1). These objectives more accurately reflect the lipid composition of adipose tissue rather than the lipid droplet objective from iAdipocytes1809 and iAdipocytes1850, which was based on isolated lipid droplets from Chinese hamster ovary (CHO) cells (Table S1). These objectives were then maximized to yield new tissue-specific fluxes.

Since ammonia is a byproduct of amino acid catabolism (Walker, 2009), we then compared brown and white adipocyte fluxes in amino acid metabolism. This comparison suggested that the largest differences in amino acid metabolism would involve ornithine-related pathways (Figure 3A) and potentially urea secretion (Figure 3B). Thus, to determine if brown compared to white adipocytes may preferentially secrete excess nitrogenous waste as urea instead of ammonia, we examined a gene expression dataset (GEO GSE27657) comparing brown to white adipose tissue (Svensson et al., 2011) and found a 3-fold higher expression of arginase 2, the enzyme that catalyzes the formation of urea and ornithine (Figure 3C). We directly measured urea flux and, consistent with the difference in gene expression, urea secretion was higher in brown compared to white adipocytes (Figure 3D). Brown adipocytes, but not white adipocytes, showed a dose-dependent response of ADIPOQ and UCP1 to the arginase inhibitor ABH during adipogenesis (Figure 3E), suggesting a functional importance of urea production specific to brown adipocytes.

Integrating Seahorse and Nova Analyzer profiles with Recon 2.1A enables prediction of flux differences

After optimizing the lipid profiles subject to the constraints of flux balance, nutrient uptake, and extracellular flux measurements, some reactions could still carry a range of flux. Thus, under these conditions, we applied flux variability analysis (Mahadevan and Schilling, 2003) (FVA) to probe the maximum and minimum feasible flux every reaction could carry in brown or in white adipocytes. FVA yielded 85 reactions with non-overlapping flux ranges between brown and white adipocytes (Table S1). Figure 4A illustrates the top 30 non-overlapping ranges of these reactions. The non-overlapping fluxes were enriched in metabolic pathways largely related to central metabolism and metabolism of specific amino acids (Figure 4B). Each non-overlapping reaction is likely to have a role in distinguishing brown and white adipocytes, such as 4-aminobutyrate (GABA) transaminase (Figure 4C). GABA, one of the reactants of this reaction, was found to be higher in brown adipocyte lysates (Figure 4D). The enzyme catalyzing this reaction, *ABAT,* has significantly higher protein levels in brown adipocytes (Figure 4E). While the role of GABA in adipocytes is unclear, *ABAT* has been shown to be essential for mitochondrial nucleoside metabolism (Besse et al., 2015).

Key metabolic fluxes are concordant with preadipocyte and adipocyte gene expression

To further validate fluxes differentially active in brown and white adipocytes, we measured global gene expression patterns by microarray from paired brown and white preadipocytes. Then we sought indications of what fluxes are likely to be different based on what genes were differentially expressed at a threshold of FDR=0.15 (van Berlo et al., 2011). We found 35 unique genes significant at this FDR (see https://github.com/jdreyf/pread-brown-white for all probes' statistics), however only one of these was associated with a reaction in the model that could carry flux in the Seahorse media: adenylate kinase 4. We can only enforce constraints on reactions that require this gene, but according to the model the reactions associated with adenylate kinase 4 can also utilize its isozymes such as adenylate kinase 2, so this microarray dataset did not allow for any model reaction constraints. However, we did find that the gene *ABAT* was nominally significantly upregulated in brown preadipocytes (p=0.04).

Although the association between gene expression and metabolic flux is generally weak and varies depending on the subsystem (which is akin to a pathway) under study (Chubukov et al., 2013), we took a second gene expression approach to validate our model. We compared predicted flux differences to the differences in associated gene expression between brown and white adipose tissue from the gene expression dataset GEO GSE27657. We observed high concordance between the direction of gene expression change and the direction of predicted flux magnitude change in several subsystems, including the citric acid cycle, cholesterol metabolism, and branched-chain amino acid (BCAA) metabolism (Figure S5). Many of these results are largely consistent with the significant subsystems revealed by enrichment of the non-overlapping fluxes without gene expression (Figure 4B), but a few subsystems are not consistent, such as histidine and methionine/cysteine metabolism.

Discussion

Several advances were made in this work. First, we reconstructed Recon 2.1A such that it was suitable for FBA by revising Recon 2.1x. Recon 2.1x is a revision of Recon 2 that has substantially more lipid metabolism reactions (Smallbone, 2013), but we had to revise Recon 2.1x due to several key biologically unrealistic predictions, such as unreasonably high ATP production with limited oxygen and nutrients. During the time we were working on this project, Recon 2.2 was published (Swainston et al., 2016). However, Recon 2.2 is not based on Recon 2.1x, thus, Recon 2.2 is less comprehensive regarding lipid metabolism important to brown and white adipocytes.

Secondly, and more importantly, the results presented here demonstrate that in adipocytes many fluxes can be sufficiently constrained to reveal intracellular metabolic differences from measurements of oxygen consumption and extracellular acidification when the nutrient media is known. Knowledge of the nutrient media allowed us to bound uptake by assuming that nutrients were not depleted from the media over the three hour assay interval. If this assumption was flawed, it could explain why Recon 2.1A could not produce feasible solutions when integrating the sodium or potassium flux measurements. The other potential reason is that some reactions involving potassium and sodium in the model may be incorrect, e.g. the model may need additional co-transport reactions for each of potassium and sodium.

The brown and white adipose tissue substrate preference for energy utilization and adipose tissue development is unclear (Montanari et al., 2017). Higher uptake of glucose, glutamine, and palmitate was measured in brown adipocytes compared to white adipocytes, which is consistent with the notion that higher energy expenditure is accompanied with higher overall substrate flux. In contrast, ammonia secretion, one of the metabolites of amino acid catabolism, was higher in white adipocytes. We find that this discrepancy is resolved by the observation that brown adipocytes have higher rates of urea production. The higher secretion of urea may be due to higher levels of arginase-2 (ARG2), a mitochondrial arginase isozyme known to be involved in pathways beyond ureagenesis including the synthesis of polyamines (Wu and Morris, 1998), which are critical for adipogenesis (Brenner et al., 2015). Arginine, the substrate for ARG2 that is converted to urea and ornithine, has been suggested to increase brown adipose tissue activity (McKnight et al., 2010). Differentiating preadipocytes treated with the arginase inhibitor ABH increased UCP1 and ADIPOQ expression in brown

adipocytes, but not white adipocytes. Thus, flux through ARG2 in brown adipose tissue has functional importance and may be a target to shift the metabolic profile to a more brown-like state.

Many methods have been developed to infer flux from common omics technologies by integrating with genome-scale modeling (Lewis et al., 2012; Shlomi et al., 2008), but the data from these technologies has only a weak association to flux, whereas extracellular flux measurements directly constrain the flux space. After accounting for constraints from the nutrient media, incorporating Seahorse measurements affects the bounds of over 10,000 reactions. In contrast, to properly estimate a reaction's flux from non-flux data, one needs kinetic parameters and quantitative estimates of the concentrations of active enzyme and all products and reactants. Gene expression from microarrays or RNA-seq, for example, falls short of this. The weak association between gene expression and flux is one reason we did not use gene expression to reconstruct brown and white adipocyte specific models; another reason is that gene expression datasets are context-specific, whereas cell-type specific models ought to include the reactions a cell can carry out in any context. Even though we did not reconstruct a cell-type specific model, we still selected an objective for modeling despite this being a known challenge for human cells. Adipocytes, under certain conditions (Berry et al., 2014), are lipid-laden cells whose expansion is characterized by de novo lipogenesis, thus we defined a lipid objective. Combining this objective with network-wide gene expression can point to more likely flux configurations, though, and it is reassuring that in key pathways, such as the citric acid cycle, where expression and flux were concordant in lower organisms (Chubukov et al., 2013), gene expression differences of brown compared to white adipocytes are consistent with our predicted flux differences.

One strategy to metabolically reprogram white adipocyte metabolism to more closely resemble that of brown adipocytes is to target UCP1 activity (Xue et al., 2015), but here we identify many other enzymes that catalyze reactions likely to be different between white compared to brown adipocytes, which are also candidate targets for reprogramming. More generally, one could search for candidate reactions for metabolic reprogramming between any two metabolic profiles. Going forward, the combination approach of metabolic flux profiling and quantitative flux modeling described here can be applied to other tissues, such as liver, brain, and skeletal muscle (Bordbar et al., 2011; Gavai et al., 2015; Nogiec et al., 2015), and it can similarly be extended to any cell type assayed with extracellular analyzers, such as cancer vs. normal cells, stem cells vs. differentiated cells, and treated vs. untreated cells. Thus, we have released a freely available R software package, *sybilxf*, based on the R package *Sybil* (Gelius-Dietrich et al., 2013), to perform metabolic modeling and search for predicted differences between metabolic profiles produced by the Seahorse Analyzer.

Experimental Procedures

Comprehensive descriptions of these methods and others are available at Supplemental Experimental Procedures.

Cell culture

Human immortalized white and brown preadipocyte cell lines were obtained from normal subjects and cultured as previously described (Xue et al., 2015).

Assessment of statistically significant flux differences between brown and white adipocytes

To calculate a flux distribution for each of brown and white adipocytes in Recon 2.1A from the Analyzer data, we sampled from the Analyzer data. We then compared brown and white adipocyte fluxes statistically.

Microarray analysis of preadipocytes

Paired differential expression analysis between brown and white samples assayed with GeneChip PrimeView (Affymetrix, Santa Clara, CA) arrays was performed in *limma* (Ritchie et al., 2015).

Supplementary Material

Refer to Web version on PubMed Central for supplementary material.

Acknowledgments

The authors would like to thank Katia Oleinik for high performance computing technical assistance; Mark Crovella for suggested analyses; Marcia Haigis and Elma Zaganjor for the Nova instrument; Jens Nielsen for providing iAdipocytes1850; Neil Swainston for clarifications on Recon 2.2; Jonathan Fritzemeier for help with the *Sybil* package; and the Joslin Diabetes Center Media Core, supported by P30DK036836 (to Joslin's Diabetes Research Center, DRC). AKR was supported by NIH grant T32 DK007260-37. This work was supported in part by NIH grants R01DK082659 (to CRK), R01DK077097 and R01DK102898 (to Y-HT), and the Joslin Diabetes Center DRC Grant P30DK036836. MDL was supported by NIH grants T32DK007260, F32DK102320 and K01DK111714.

References

Aurich MK, Paglia G, Rolfsson Ó, Hrafnsdóttir S, Magnúsdóttir M, Stefaniak MM, Palsson B, Fleming RMT, Thiele I. Prediction of intracellular metabolic states from extracellular metabolomic data. Metabolomics. 2015; 11:603–619. [PubMed: 25972769]

Berbée JFP, Boon MR, Khedoe PPSJ, Bartelt A, Schlein C, Worthmann A, Kooijman S, Hoeke G, Mol IM, John C, et al. Brown fat activation reduces hypercholesterolaemia and protects from atherosclerosis development. Nat Commun. 2015; 6:6356. [PubMed: 25754609]

van Berlo RJP, de Ridder D, Daran JM, Daran-Lapujade PaS, Teusink B, Reinders MJT. Predicting metabolic fluxes using gene expression differences as constraints. IEEE/ACM Trans Comput Biol Bioinform. 2011; 8:206–216. [PubMed: 21071808]

Berry R, Jeffery E, Rodeheffer MS. Weighing in on adipocyte precursors. Cell Metab. 2014; 19:8–20. [PubMed: 24239569]

Besse A, Wu P, Bruni F, Donti T, Graham BH, Craigen WJ, McFarland R, Moretti P, Lalani S, Scott KL, et al. The GABA transaminase, ABAT, is essential for mitochondrial nucleoside metabolism. Cell Metab. 2015; 21:417–427. [PubMed: 25738457]

Bordbar A, Feist AM, Usaite-Black R, Woodcock J, Palsson BO, Famili I. A multi-tissue type genome-scale metabolic network for analysis of whole-body systems physiology. BMC Syst Biol. 2011; 5:180. [PubMed: 22041191]

Brenner S, Bercovich Z, Feiler Y, Keshet R, Kahana C. Dual Regulatory Role of Polyamines in Adipogenesis. J Biol Chem. 2015; 290:27384–27392. [PubMed: 26396188]

Cannon JBN. Brown adipose tissue: Function and physiological significance. Physiol Rev. 2004; 84:277–359. [PubMed: 14715917]

Chelliah V, Juty N, Ajmera I, Ali R, Dumousseau M, Glont M, Hucka M, Jalowicki G, Keating S, Knight-Schrijver V, et al. BioModels: Ten-year anniversary. Nucleic Acids Res. 2015; 43:D542–D548. [PubMed: 25414348]

Chubukov V, Uhr M, Le Chat L, Kleijn RJ, Jules M, Link H, Aymerich S, Stelling J, Sauer U. Transcriptional regulation is insufficient to explain substrate-induced flux changes in Bacillus subtilis. Mol Syst Biol. 2013; 9:709. [PubMed: 24281055]

Coles L, Rutherfurd S, Moughan P. A model to predict the ATP equivalents of macronutrients absorbed from food. Food Funct. 2013; 4:432–442. [PubMed: 23233079]

Cypess AM, Lehman S, Williams G, Tal I, Rodman D, Goldfine AB, Kuo FC, Palmer EL, Tseng YH, Doria A, et al. Identification and importance of brown adipose tissue in adult humans. N Engl J Med. 2009; 360:1509–1517. [PubMed: 19357406]

Cypess AM, White AP, Vernochet C, Schulz TJ, Xue R, Sass Ca, Huang TL, Roberts-Toler C, Weiner LS, Sze C, et al. Anatomical localization, gene expression profiling and functional characterization of adult human neck brown fat. Nat Med. 2013; 19:635–639. [PubMed: 23603815]

Cypess AM, Weiner LS, Roberts-Toler C, Elía EF, Kessler SH, Kahn PA, English J, Chatman K, Trauger SA, Doria A, et al. Activation of human brown adipose tissue by a β3-adrenergic receptor agonist. Cell Metab. 2015; 21:33–38. [PubMed: 25565203]

Dreyfuss JM, Zucker JD, Hood HM, Ocasio LR, Sachs MS, Galagan JE. Reconstruction and Validation of a Genome-Scale Metabolic Model for the Filamentous Fungus Neurospora crassa Using FARM. PLoS Comput Biol. 2013:9.

Fan J, Kamphorst JJ, Mathew R, Chung MK, White E, Shlomi T, Rabinowitz JD. Glutamine-driven oxidative phosphorylation is a major ATP source in transformed mammalian cells in both normoxia and hypoxia. Mol Syst Biol. 2013; 9:712. [PubMed: 24301801]

Fan J, Ye J, Kamphorst JJ, Shlomi T, Thompson CB, Rabinowitz JD. Quantitative flux analysis reveals folate-dependent NADPH production. Nature. 2014; 510:298–302. [PubMed: 24805240]

Feist AM, Herrgård MJ, Thiele I, Reed JL, Palsson BØ. Reconstruction of biochemical networks in microorganisms. Nat Rev Microbiol. 2009; 7:129–143. [PubMed: 19116616]

Frezza C, Zheng L, Folger O, Rajagopalan KN, MacKenzie ED, Jerby L, Micaroni M, Chaneton B, Adam J, Hedley A, et al. Haem oxygenase is synthetically lethal with the tumour suppressor fumarate hydratase. Nature. 2011; 477:225–228. [PubMed: 21849978]

Gavai AK, Supandi F, Hettling H, Murrell P, Jack A. Using Bioconductor Package BiGGR for Metabolic Flux Estimation Based on Gene Expression Changes in Brain. 2015:1–21.

Gelius-Dietrich G, Desouki AA, Fritzemeier CJ, Lercher MJ. Sybil--efficient constraint-based modelling in R. BMC Syst Biol. 2013; 7:125. [PubMed: 24224957]

Gesta S, Bezy O, Mori MA, Macotela Y, Lee KY, Kahn CR. Mesodermal developmental gene Tbx15 impairs adipocyte differentiation and mitochondrial respiration. Proc Natl Acad Sci U S A. 2011; 108:2771–2776. [PubMed: 21282637]

Giralt M, Villarroya F. White, brown, beige/brite: different adipose cells for different functions? Endocrinology. 2013; 154:2992–3000. [PubMed: 23782940]

Hanssen MJW, Hoeks J, Brans B, van der Lans AAJJ, Schaart G, van den Driessche JJ, Jörgensen JA, Boekschoten MV, Hesselink MKC, Havekes B, et al. Short-term cold acclimation improves insulin sensitivity in patients with type 2 diabetes mellitus. Nat Med. 2015; 21:863–865. [PubMed: 26147760]

Harms M, Seale P. Brown and beige fat: development, function and therapeutic potential. Nat Med. 2013; 19:1252–1263. [PubMed: 24100998]

Hoene M, Li J, Häring HU, Weigert C, Xu G, Lehmann R. The lipid profile of brown adipose tissue is sex-specific in mice. Biochim Biophys Acta - Mol Cell Biol Lipids. 2014; 1841:1563–1570.

Holzhütter HG. The principle of flux minimization and its application to estimate stationary fluxes in metabolic networks. Eur J Biochem. 2004; 271:2905–2922. [PubMed: 15233787]

Hyvönen MT, Spalding KL. Maintenance of white adipose tissue in man. Int J Biochem Cell Biol. 2014; 56:123–132. [PubMed: 25240584]

Kaplon J, Zheng L, Meissl K, Chaneton B, Selivanov Va, Mackay G, Burg SH, Van Der Verdegaal EME, Cascante M, Shlomi T, et al. A key role for mitochondrial gatekeeper pyruvate dehydrogenase in oncogene-induced senescence TL - 498. Nature. 2013; 498 VN:109–112. [PubMed: 23685455]

Laakso M, Kuusisto J. Insulin resistance and hyperglycaemia in cardiovascular disease development. Nat Rev Endocrinol. 2014; 10:293–302. [PubMed: 24663222]

Lewis NE, Nagarajan H, Palsson BØ. Constraining the metabolic genotype-phenotype relationship using a phylogeny of in silico methods. Nat Rev Microbiol. 2012; 10:291–305. [PubMed: 22367118]

Mahadevan R, Schilling CH. The effects of alternate optimal solutions in constraint-based genome-scale metabolic models. Metab Eng. 2003; 5:264–276. [PubMed: 14642354]

Mardinoglu A, Kampf C, Asplund A, Fagerberg L, Hallström BM, Edlund K, Blüher M, Pontén F, Uhlen M, Nielsen J. Defining the human adipose tissue proteome to reveal metabolic alterations in obesity. J Proteome Res. 2014; 13:5106–5119. [PubMed: 25219818]

Mardinoglu A, Heiker JT, Gärtner D, Björnson E, Schön MR, Flehmig G, Klöting N, Krohn K, Fasshauer M, Stumvoll M, et al. Extensive weight loss reveals distinct gene expression changes in human subcutaneous and visceral adipose tissue. Sci Rep. 2015; 5:14841. [PubMed: 26434764]

Mardinoglu, a, Agren, R., Kampf, C., Asplund, A., Nookaew, I., Jacobson, P., Walley, aJ, Froguel, P., Carlsson, LM., Uhlen, M., et al. Integration of clinical data with a genome-scale metabolic model of the human adipocyte. Mol Syst Biol. 2013; 9:649–649. [PubMed: 23511207]

McKnight JR, Satterfield MC, Jobgen WS, Smith SB, Spencer TE, Meininger CJ, McNeal CJ, Wu G. Beneficial effects of l-arginine on reducing obesity: potential mechanisms and important implications for human health. Amino Acids. 2010; 39:349–357. [PubMed: 20437186]

Mo ML, Palsson BØ, Herrgard MJ. Connecting extracellular metabolomic measurements to intracellular flux states in yeast. BMC Syst Biol. 2009; 3:37. [PubMed: 19321003]

Montanari T, Pošćić N, Colitti M. Factors involved in white-to-brown adipose tissue conversion and in thermogenesis: a review. Obes Rev. 2017

Munger J, Bennett BD, Parikh A, Feng XJJ, McArdle J, Rabitz Ha, Shenk T, Rabinowitz JD. Systems-level metabolic flux profiling identifies fatty acid synthesis as a target for antiviral therapy. Nat Biotechnol. 2008; 26:1179–1186. [PubMed: 18820684]

Nogiec C, Burkart A, Dreyfuss JM, Lerin C, Kasif S, Patti ME. Metabolic modeling of muscle metabolism identifies key reactions linked to insulin resistance phenotypes. Mol Metab. 2015; 4:151–163. [PubMed: 25737951]

Orgel E, Mittelman SD. The links between insulin resistance, diabetes, and cancer. Curr Diab Rep. 2013; 13:213–222. [PubMed: 23271574]

Orth JD, Thiele I, Palsson BØ. What is flux balance analysis? Nat Biotechnol. 2010; 28:245–248. [PubMed: 20212490]

Quek LE, Dietmair S, Krömer JO, Nielsen LK. Metabolic flux analysis in mammalian cell culture. Metab Eng. 2010; 12:161–171. [PubMed: 19833223]

Quek LE, Dietmair S, Hanscho M, Martínez VS, Borth N, Nielsen LK. Reducing Recon 2 for steady-state flux analysis of HEK cell culture. J Biotechnol. 2014; 184:172–178. [PubMed: 24907410]

Ritchie ME, Phipson B, Wu D, Hu Y, Law CW, Shi W, Smyth GK. limma powers differential expression analyses for RNA-sequencing and microarray studies. 2015:43.

Sahoo S, Haraldsdóttir HS, Fleming RMT, Thiele I. Modeling the effects of commonly used drugs on human metabolism. FEBS J. 2015; 282:297–317. [PubMed: 25345908]

Sanchez-Gurmaches J, Guertin Da. Adipocyte lineages: Tracing back the origins of fat. Biochim Biophys Acta. 2013

Shlomi T, Cabili MN, Herrgård MJ, Palsson BØ, Ruppin E. Network-based prediction of human tissue-specific metabolism. Nat Biotechnol. 2008; 26:1003–1010. [PubMed: 18711341]

Si Y, Shi H, Lee K. Impact of perturbed pyruvate metabolism on adipocyte triglyceride accumulation. Metab Eng. 2009; 11:382–390. [PubMed: 19683593]

Smallbone, K. Striking a balance with Recon 2.1. 2013. p. 14-17.

Svensson PA, Jernås M, Sjöholm K, Hoffmann JM, Nilsson BE, Hansson M, Carlsson LMS. Gene expression in human brown adipose tissue. Int J Mol Med. 2011; 27:227–232. [PubMed: 21125211]

Swainston N, Smallbone K, Hefzi H, Dobson P, Brewer J, Hanscho M, Zielinski D, Ang K, Gardiner N, Gutierrez J, et al. Recon 2.2: from reconstruction to model of human metabolism. Metabolomics. 2016

Tchkonia T, Thomou T, Zhu Y, Karagiannides I, Pothoulakis C, Jensen MD, Kirkland JL. Mechanisms and metabolic implications of regional differences among fat depots. Cell Metab. 2013; 17:644–656. [PubMed: 23583168]

Thiele I, Palsson BØ. A protocol for generating a high-quality genome-scale metabolic reconstruction. Nat Protoc. 2010; 5:93–121. [PubMed: 20057383]

Thiele I, Swainston N, Fleming RMT, Hoppe A, Sahoo S, Aurich MK, Haraldsdottir H, Mo ML, Rolfsson O, Stobbe MD, et al. A community-driven global reconstruction of human metabolism. Nat Biotechnol. 2013; 31:419–425. [PubMed: 23455439]

Tran TT, Kahn CR. Transplantation of adipose tissue and stem cells: role in metabolism and disease. Nat Rev Endocrinol. 2010; 6:195–213. [PubMed: 20195269]

Tseng YH, Cypess AM, Kahn CR. Cellular bioenergetics as a target for obesity therapy. Nat Rev Drug Discov. 2010; 9:465–482. [PubMed: 20514071]

Walker V. Ammonia toxicity and its prevention in inherited defects of the urea cycle. Diabetes, Obes Metab. 2009; 11:823–835. [PubMed: 19531057]

Wu G, Morris SM. Arginine metabolism: nitric oxide and beyond. Biochem J. 1998; 336:1–17. [PubMed: 9806879]

Xue R, Lynes MD, Dreyfuss JM, Shamsi F, Schulz TJ, Zhang H, Huang TL, Townsend KL, Li Y, Takahashi H, et al. Clonal analyses and gene profiling identify genetic biomarkers of the thermogenic potential of human brown and white preadipocytes. Nat Med. 2015; 21:760–768. [PubMed: 26076036]

A

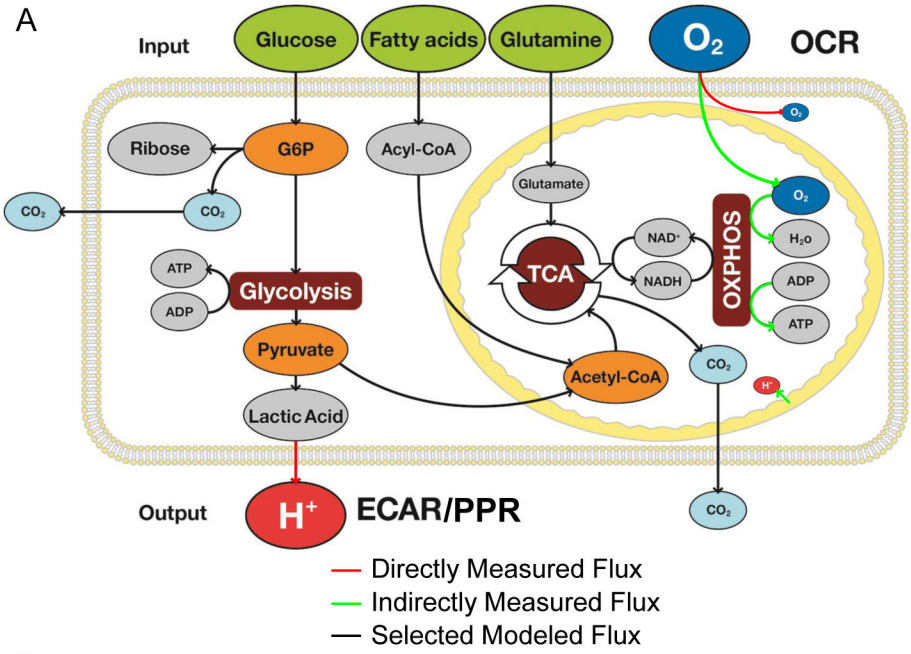

B

Indirectly Measured Flux	Equation
ATP Production	$OCR_{basal} - OCR_{oligo}$
Mitochondrial Respiration	$OCR_{basal} - OCR_{rotenone}$
Non-mitochondrial Respiration	$OCR_{rotenone}$
Proton Leak	$OCR_{oligo} - OCR_{rotenone}$
Spare Respiratory Capacity	$OCR_{FCCP} - OCR_{basal}$

Figure 1. Schematic representation of integrative modeling

(A) The Seahorse XF Analyzer directly measures oxygen consumption rate (OCR) and extracellular acidification rate/proton production rate (ECAR/PPR) (red), indirectly measures intracellular fluxes through chemical perturbations such as oligomycin and rotenone (green), other fluxes are modeled via metabolic modeling and may be predicted (selected fluxes shown in black). (B) Table explaining how indirectly measured fluxes are calculated from Seahorse measurements. See also Table S2.

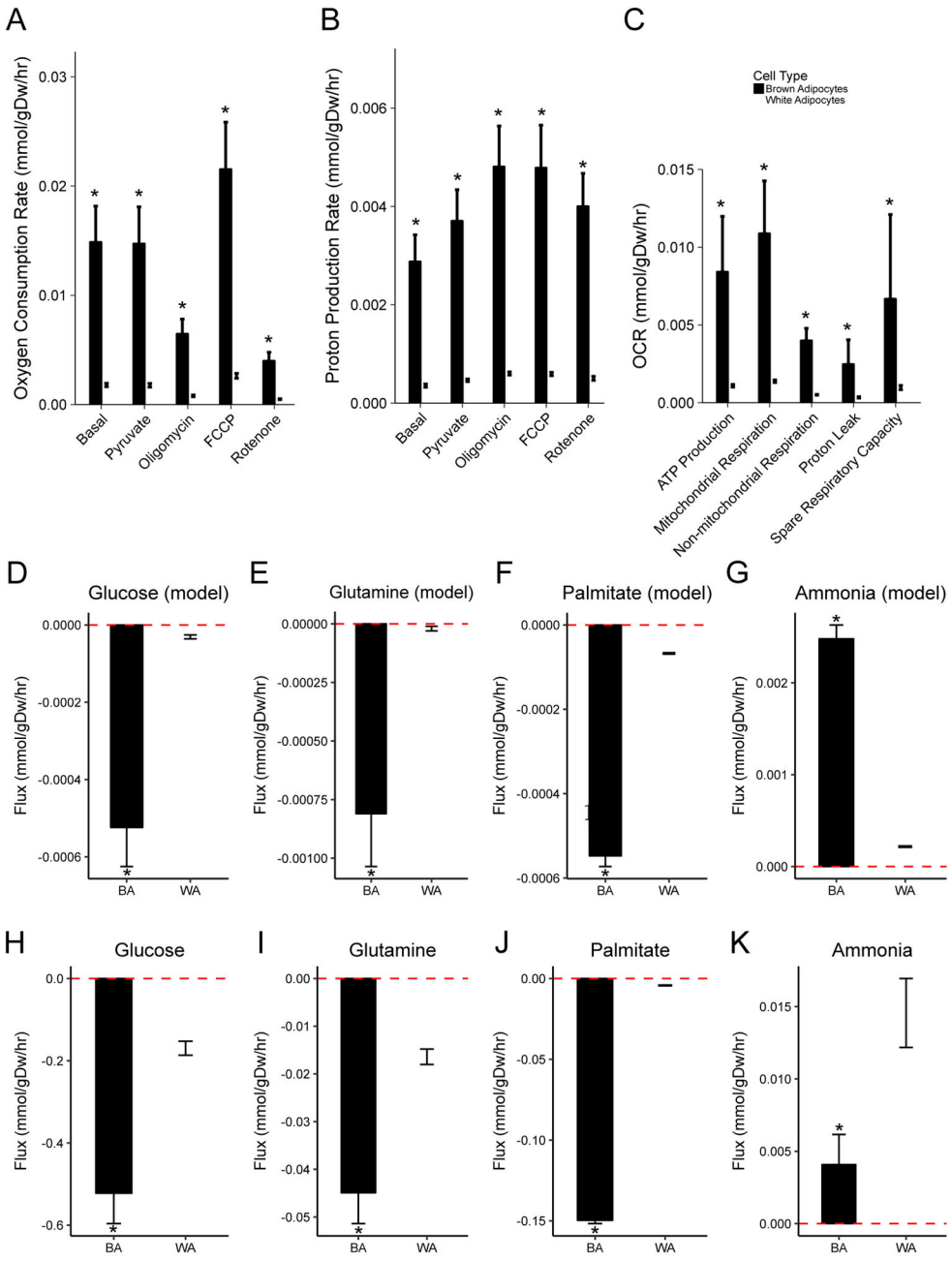

Figure 2. Measured, predicted, and validated fluxes on brown and white adipocyte Seahorse extracellular flux profiles

Oxygen consumption rates (A) and proton production rates (B) were measured in response to pyruvate, oligomycin (an ATP synthase inhibitor), FCCP (a mitochondrial de-coupler), and rotenone (a Complex I inhibitor). Brown adipocytes (black), compared to white adipocytes (white), showed significantly higher rates of oxygen consumption and extracellular acidification (proton production) under every injection. (C) Indirectly measured fluxes as revealed by differences in oxygen consumption rates. These extracellular flux profiles of brown and white adipocytes were integrated into the model by sampling from the

data and minimizing total flux. The model predicted higher glucose, glutamine, and palmitate uptake and higher ammonia secretion for brown adipocytes (D–G). Experimentally measuring these metabolites showed consistent results for glucose, glutamine, and palmitate (H–J), but not for ammonia (K). Bars indicate mean ± s.e.m. Seahorse measurements were normalized to DNA; Nova measurements were normalized to protein; units were converted to dry weight. See also Figures S3 and S4.

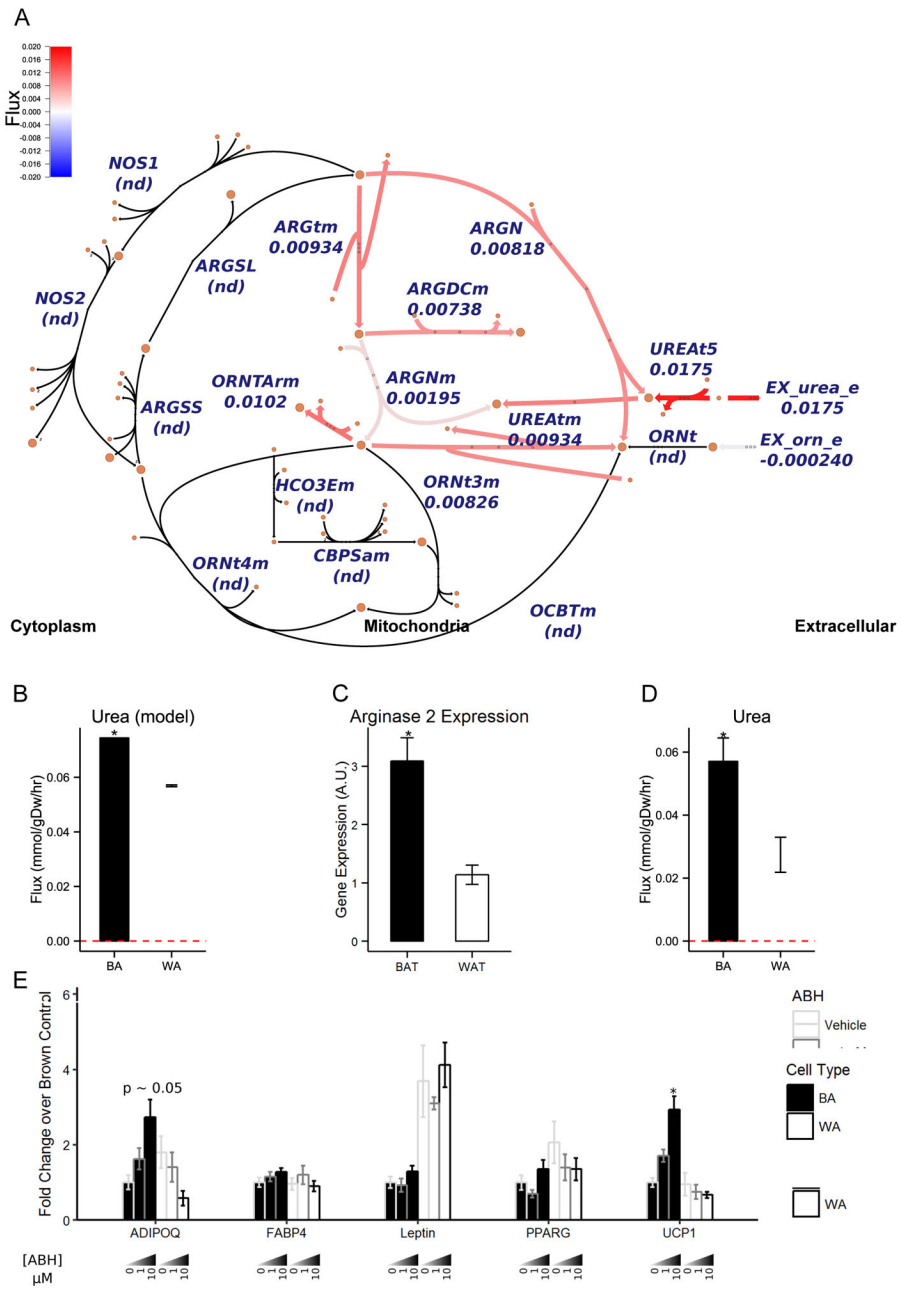

Figure 3. Amino acid metabolism in brown and white adipocytes

(A) The differences between brown and white predicted fluxes in amino acid catabolism. Red = higher in brown adipocytes, blue = higher in white, black = neither brown nor white adipocytes carried flux through those reactions. (B) The model predicted higher secretion of urea. (C) Gene expression showed approximately a 3-fold higher expression of arginase 2 in brown adipose tissue compared to white adipose tissue. (D) Urea flux was higher in brown adipocytes compared to white adipocytes. Bars indicate mean ± s.e.m. (E) Inhibiting arginase activity via the chemical ABH altered several key adipogenic genes in brown adipocytes, but not white adipocytes.

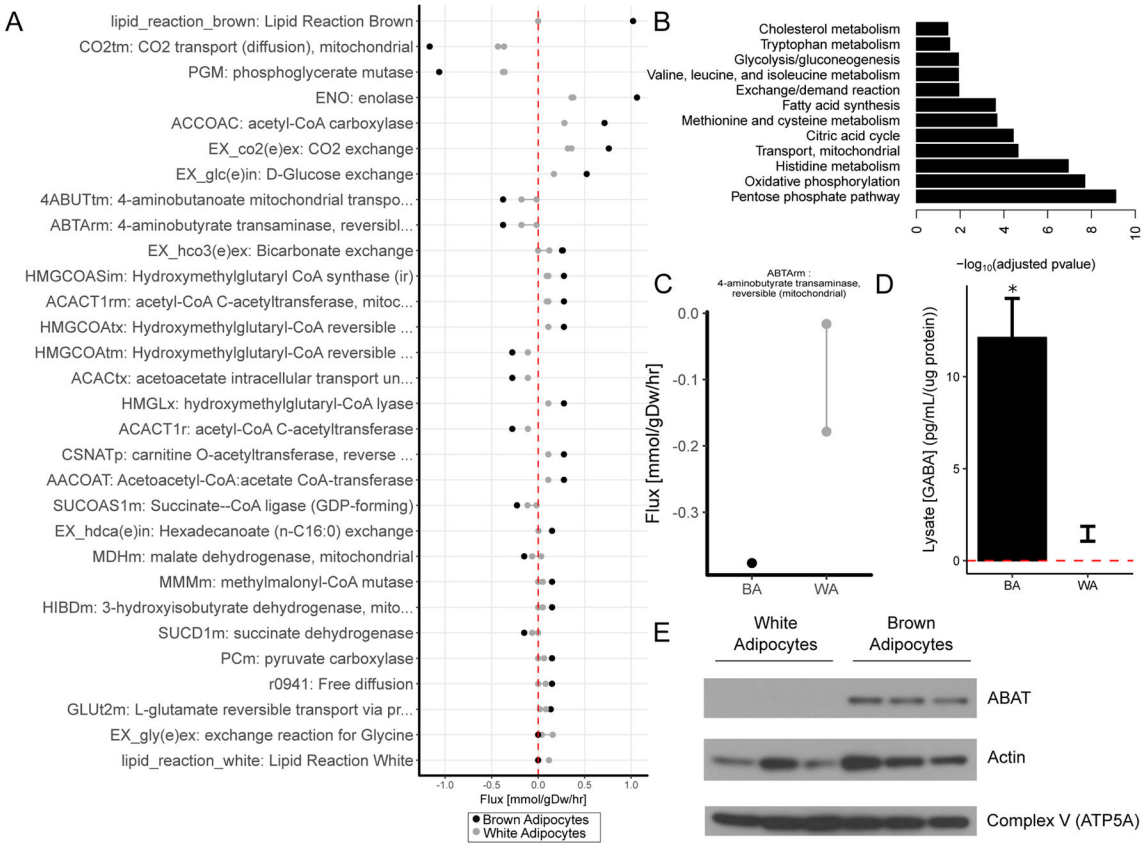

Figure 4. Reactions predicted to have non-overlapping flux ranges between brown and white adipocytes

(A) Top 30 reactions as revealed by flux variability analysis whose predicted extrema did not overlap between brown and white adipocytes. See also Table S1. (B) The non-overlapping reactions were enriched in pathways related to central metabolism and amino acid metabolism, as shown by their -$\log_{10}$(FDR). See also Figure S5, where flux predictions are compared to gene expression by pathway. These reactions are likely to have some distinguishing role in brown and white adipocyte biology, such as 4-aminobutyrate transaminase (C) in mitochondrial maintenance. The reactant metabolite GABA (D) and the catalyzing gene *ABAT* (E) were found to be higher in brown adipocytes.